Original Article

Biochemistry properties of Platinum nanoparticles and Adatoms

Ahmad Khalaf Alkhawaldeh
Department of Allied medical sciences, Zarqa University College, Al-Balqa Applied University, Jordan
Email: ahmad.khawaldeh@bau.edu.jo
DOI: 10.47750/pnr.2023.14.03.153

Abstract

Dielectric constants, dielectric degradation and A.C. conductivity have been calculated according to the doping material frequency and composition. High AC-conductivity and low dielectric constant were observed at higher frequencies. The above hypothesis can be clarified by 'Maxwell Wagner Model' and may offer new insights into the manufacture of dialectically conceivable nanomaterials. The degradation of Rhoda mine B in the UV visible light has been investigated for the photocatalytic function of our samples. The analysis of photocatalyst provides a convenient way to determine your destiny by various reutilizations.

Keywords: Biochemistry; Williamson-Hall; Scanning Electron Microscope (SEM); Particle; Analyzer.

1. INTRODUCTION

Normally, the unwanted Platinum exhibits n-type conductivity that is normally attributed to native defects including the absence of oxygen and interstitial titanium. Modifying Platinum by metal/non-metal doping can affect the process of crystallization (size, shape, morphology, porosity and stability) dramatically improve microstructural, electric and optical properties drastically by creating mid band gap electronic states that interfere with the host electrons and alter the host electronic states [1]. The recent study explains the effect of impurities on the dielectrically efficiency of Platinum It is clear that the decrease in dielectric constant as coulomb interaction between the electron and the hole increases the energy of excitonic binding which is ideal for applications in the optoelectronic fields [2, 3]. Also delighted to study the photocatalytic activity of Platinum corresponding to UV visible light. However, it still under discussion and the structure as well as the function of various reactive oxygen species (ROS) and the presence of crystal defect chemistry, such as the presence of oxygen vacancies (VO) and the reduction of titanium ions ($Ti^{4+} \rightarrow Ti^{3+}$) still unclear. In addition, the dopants content reduce recombination levels of electron–hole pair photo generated in Platinum. Metal ions have been studied; including iron, chromium; manganese and cobalt were introduced into titanium to ameliorate the electronic energy band structure [4-6]. In addition, doping non-metal (rare earth RE) Platinum nanoparticles improves the stability of the anatase process and avoids separation from phase. RE ions are often named for their complex structure by different Lewis bases, e.g. acids, alcohols. These Lewis bases interact with the f-orbitals via their functional groups [7]. The incorporation of these ions within a Platinum matrix will provide a way to concentrate molecular pollutants on the semiconductor surface and, as a recombination center, increase the activity of the photography. On the other hand, photocatalyst Er in Platinum generated with Sol-gel method recorded improved photocatalytic degradation in phenol dye by a doping of 2 wt percent [8, 9]. Prepared RE nanoparticles Platinum , doped by a solvothermal pathway, it concluded that near-infrared or visual light can be converted to visible and UV light by doped rare earth Er^{3+}, which enhances the photocatalytic action of Platinum [10]. The remarkable application in optoelectronic devices and flat panel displays, the core study of the RE elements hosted in semiconductor materials are though provoking. Beside of their special illumination, rare earth-doped luminescent materials have drawn great attention due to their unique luminescent properties coming from the intra 4f and 4f–5d transitions [11, 12]. Furthermore, A wide range of structure-directing agents such as ionic liquid, poly (ethylene glycol), diblock copolymer, triblock copolymers (P123), hexadecylamine and cetyltrimethylammonium bromide (CTAB) have been used to prepare the porous titanium oxide. Steric and/or electrostatic forces may help make these structures stable such that the particles are kept separate [13]. The key goal was for the surface atoms to passive, by increasing the surfactant's surface-free energy (CTAB). For titanium consisting of "weak" cat ions Ti^{4+}, which bind to oxygen through strong ties [14]. In the work, discussed surfactants may perform certain functions, as modifier agent to slow the formation of the titanium lattice. Normally, Nano sized semiconductor Platinum produce a significant number of surface oxygen vacancies due to the effect on the surface as well as the size effects. The

oxygen vacancies have intense effect on the electronic states. The effect on material characteristics of oxygen vacancies is therefore a critical factor in various applications. Several techniques for improving the photocatalytic activities have been studied, such as the size of the crystal, the surface and the facet-controlled morphologies, which enable electrons or holes to move rapidly and to move to the surface reaction site.

2. Experimental

Unhoped and adatoms doped nanoparticles Platinum crystal structures with CuKα radiation were studied using the analysis X-ray diffractometer (k= 1.54056 Å) in order to measure the average size of nanocrystals, internal lattice stress, and the energy densities, XRD results were compiled at 0.002° per second at slow scan pace. Both samples were scanned in the range 20-70 for the diffraction peak of (101) planes (2 pounds). Scanning of the electron microscopy, chosen field electron diffraction (SAED) pattern, parcel size analysis, high magnification surface morphology, crystallinity and sample grid distance were studied (JEOL-JEM 2010 operated at 200 kV).

The nitrogen physisorption measurements were carried out on an ASAP 2020 Micrometrics. Adsorption of nitrogen–desorption isotherms were measured at 77 kilometers after 48 hours of sample degassing at 40°C. According to the traditional Brumaire–Emmett–Teller (BET) theory, the basic area, namely SBET, for the p / p0 range was calculated=0.05–0.25. Based on the t-plot process using the Lecloux-Pirard isotherm with the approximate C constant, the microspore length, the Micro and the nanoparticles surface area, smash, were determined. Net pore capacity, Vnet, was calculated by nitrogen adsorption–de-desorption p/p0 = 0.995 adsorption branch.

In the 4000-400 cm-1 range of waven numbers, a study of Fourier transformed infrared (FTIR) was carried out using (Instrument IR-200 and KBr cells), FTIR spectrums identified the various stretch and vibrational modes associated with functional groups that occur in the samples. Platinum was developed as a nanoparticles plaster with a diameter of 28.26 mm and a thickness of 1 – 1.5 mm and a 10 t/cm uniaxial press. Pellets have been sintered for 1 hour at a temperature of 500°C. All opposite faces of the pellets have been covered to create a parallel plate condenser with silver tape. In order to guarantee the strong ohmic electrodes, the protected pellets were placed between 2 platinum plates.

Both chemicals were listed as reagents and used as approved. By diluting certain chemical compounds into Milli-Q water system), aquatic solutions had been prepared. A water solution path containing the combination of the platinum/palladium electrodes used in this work. The average volume of the sample in the electroanalytical chemical cell was 20 mL in each trial.

3. Results and Discussion

3.1. X-ray diffraction

X-ray diffraction provide details on crystalline structure, grain size and lattice strain. The X-ray diffraction spectra of unhoped and doped Eu (0-1-2-3% at) Platinum samples. The quantitative studies related to structural properties were further verified by the Rietveld refinement method using the Foolproof 2000 software package. All the diffraction peaks in the doped samples are assigned well to tetragonal anisate crystalline phase of Platinum with a reference pattern (JCPDS file No.153 0152). These results are in accordance with T.E.

In this context, there is a reduction in the anatase temperature of platinum powder to the rutile phase transition. Simulated XRD patterns are obtained by fitting the experimental data to the reference data, which distinguish between experimental and sophisticated XRD patterns, respectively; the red and black lines represent the data observed and fitted. The blue line is the contrast between the data observed and the data fitted. The refined XRD architectures complement the calculated results very well.

The structure parameters are calculated from the Rietveld refining that reflect the reliability of the analyzed results, the unit cell volume, R Braggs and the grids are calculated and the effect has been on the integration of the dopant ions in the host grid.

In addition to platinum, no impurities were detected in either secondary phases of Eu2O3, EuTiO3, which means high sample purity and confirm that, under the given test conditions, Eu is successfully included into the platinum crystal grid. Who has hypothesized the high Adatoms size (0.89 Å). The Eu2O3 surface does not replace Ti4+ (0.68 Å) but migrates instead to Platinum. This did not identify this in XRD data, which could be far below the XRD detection limit due to limited quantities.

The finished grids, volume of the cell, size of the crystallite, size of the particle and interleaving distance (d) have been

described. The unit cell expansion rate increases with Eu. It can be observed that. In the literature, there was no consensus as to whether rare earth ions could substitute titanium sites in the grid or join the grid as interstitial defects. The TI replaces the Eu ions and the Ti−O connection in the platinum crystal grid has been stabilized. Our findings indicate that Eu occupied the Ti site successfully in the crystal grid. Moreover, an increase in Eu concentration leads to a drop of the sensitivity of XRD models.

3.2. Scherer method

The average crystallite size was calculated from the broadening of the (101) reflection for anatase, therefore, the Nano sized Eu doped Platinum nanoparticles varies from 17 to 12 nm and for unhoped Platinum is 28 nm (all the results are depicted in Table 1) as estimated by Scherer formula [15]:

$$D_{sc} = \frac{K\lambda}{\beta\cos\theta} \quad (1)$$

In cases where Dsc is a micro nutritional size (nm), K is a constant shape (0.9 spherical particles), β is a wavelength of x-ray (nm), and β is the maximum width of the peak chosen at half (FWHM) and Ø is the diffraction angle of the Bragg.

However, the growth of the crystallite size in platinum is impeded because of the following reasons. Replacing the major Adatoms at Ti4+ and thereby adding vacancies of oxygen would lead to the raising of the gill parameter as well as pressure, leading to a decrease in the crystallite size. In addition, several additional organic stabilizers are used and solvent itself serves as a stabilizer, making them resistant to agglomeration. The formula (Equ. (2)) determined the density of each sample [16]:

$$\rho = \frac{n * M}{N * V} \quad (2)$$

Where M is molecular, N is the number of the Avogadro and V is the unit cell length. For anatase (n = 4) and rutile (n = 2, respectively), respectively. Another relevant number was determined by formula for the particular surface area (Eq. (3)):

$$S_a = \frac{6}{D * \rho} \quad (3)$$

D is the dimension and density of the crystallite. The sampling density is very narrow. The real surface area is smaller as the doping material in Table 1 is increased. Furthermore, a delocalization is a crystal imperfect in one section of the crystal associated with the misspelling of the gate. Indeed, the mechanism for growth involving dislocation is an important matter. Dislocations are not equilibrium imperfections, in contrast to vacancies and interstices, i.e. thermodynamic attention is inadequate for their presence in the densities found. Really, the dislocation growth process is a matter from the relation (Eq.(4)) [17]:

$$\delta = \frac{1}{{D_{sc}}^2} \quad (4)$$

With the rise in crystallite size, the dislocation is found to decrease. The ionic states of Er ion differ from Ti ion, and oxygen vacancy and crystal defects are thus formed in the Platinum grid to protect load neutrality due to the load imbalance. All Rietveld refinement parameters have also been determined in Figure 1.

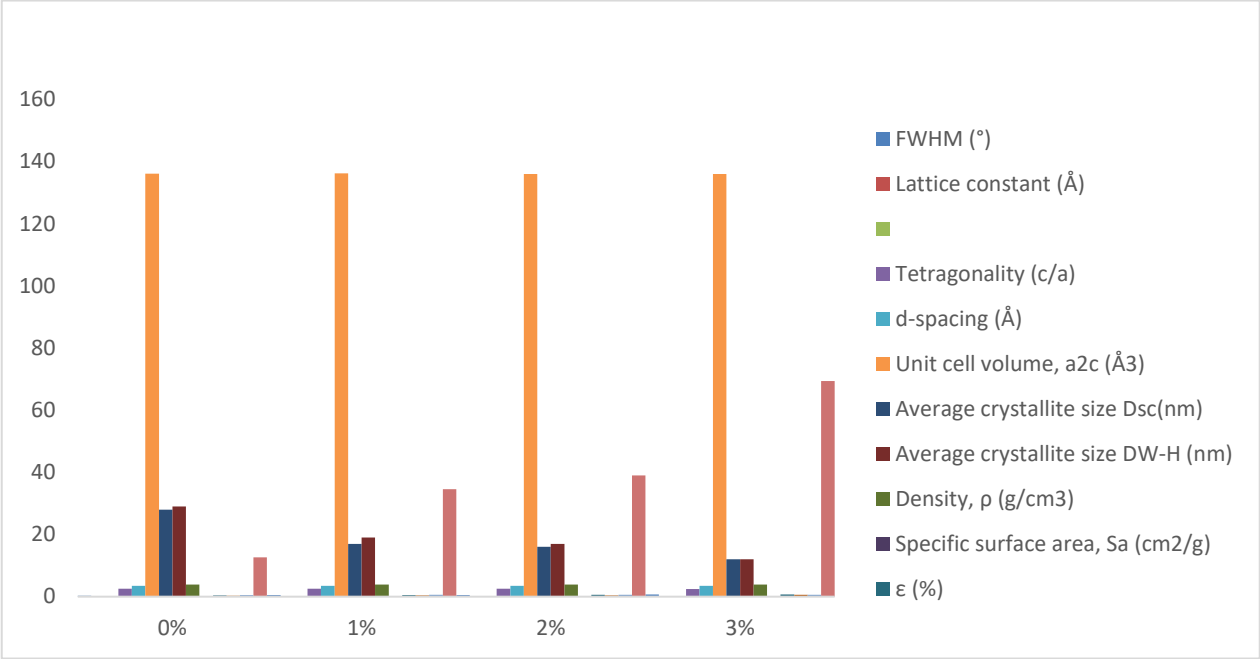

Figure 1. Refinement parameters obtained for unhoped and Eu-doped nanoparticles Platinum

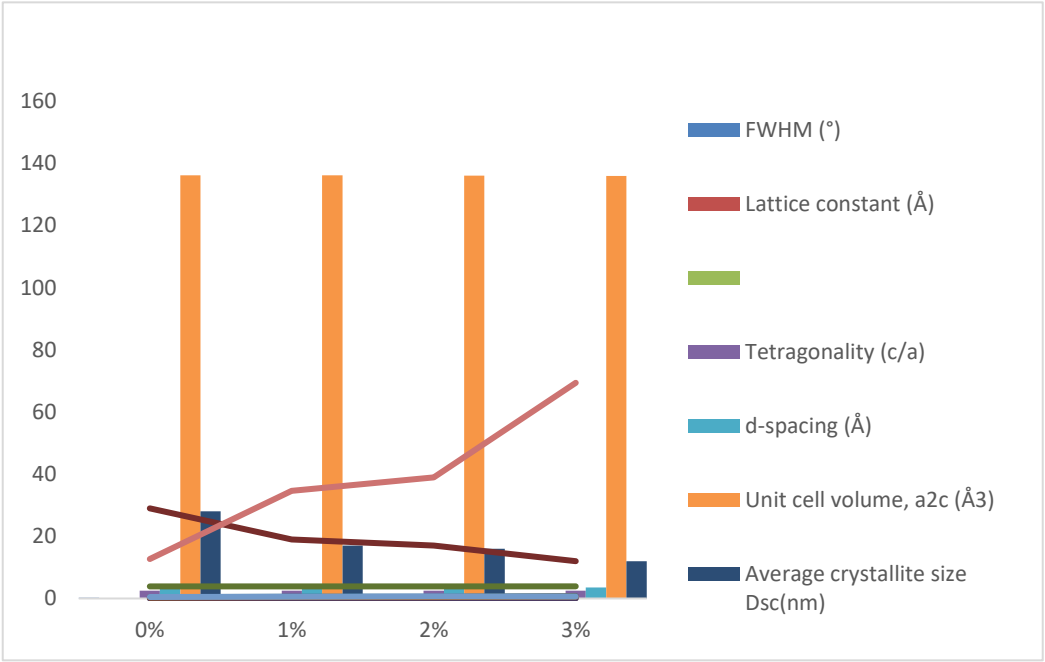

Figure 2. Refinement parameters obtained for nanoparticles Platinum

3.3. Williamson–Hall method

The lattice strain has been calculated by using the relation for Williamson–Hall plot (Eq.(5)).

$$\frac{\beta cos\theta}{\lambda} = \frac{1}{\sigma} + \frac{\eta \sin\theta}{\lambda} \quad (5)$$

β is the wavelength of x-ray while FWHM is in radials, β is the diffraction angle, β is the effective size of particles and β is the productive pressure. The process W-H does not obey the dependence of 1/cos, but differs instead with tan as in Scherer Equ. (6). this basic separation enables differentiations to be broadened as all narrow crystalline dimensions and micro-strains are combined. This disparity in strategy-discussed blow assumes that the scale and extension of stress are additive elements of a Bragg summit's overall integral FWHM width. In the study of W-H, the distinct dependence on each effect was the basis for separating the size and pressure. The detected FW was then [18].

$$\beta_{hkl} = \frac{K\lambda}{\mathrm{D}\cos\theta} + 4\varepsilon tg\theta \quad (6)$$

By rearranging

$$\beta_{hkl}\cos\theta = \frac{K\lambda}{D} + 4\varepsilon\, sin\theta \quad (7)$$

Where it is presumed that the stress is compatible in all crystallographic directions taking into consideration the isotropic character of the crystal, where the material characteristics are all independent of their path. All the experimental data points are shown in a straight line with icons and fitted data points. Table 1 displays the fitting parameters.

The positive slope in the plot indicating the presence of tensile strain. Whereas the negative slopes indicate the compressive strain. As we compared to bulk Platinum tetragonal crystal structure and synthesized Platinum a difference in lattice constants was observed in (Figure 2) for all the samples may be due to tensile strain, it is calculated using the following formula (Eq.(8)) [19]:

$$\frac{1}{d_{hkl}^2} = \frac{h^2 + k^2}{a^2} + \frac{l^2}{c^2} \quad (8)$$

Where dhkl is the separation between the leading indices of Miller, h, k, l and a and c, are the constants of the lattice. The determined structural parameters of the strongest peak (1 1 0) are seen for the samples (Table 1). In addition, the value of grid constants (a=b) and the value of grid constant (c) decrease. Due to the compressive grid pressure, this may be due. Various factors influence material tension, such as the pressure of the grid due to cracks, interlunar spacing, crystallite dimension, temperature gradients, dimensional variation and inelastic decay. The pressure caused by the spread of the peak due to distortion of the gill (micro train) Eq (9):

$$\varepsilon = \frac{\beta}{4 * tg\theta} \quad (9)$$

Furthermore, Stocks-Wilson relations (Eq.(10)) introduced another value of micro-strain along the different crystallographic planes called the root mean square (εrms) which can also be estimated by this formula:

$$\varepsilon_{rms} = \left(\frac{2}{\pi}\right)^{1/2} \varepsilon \quad (10)$$

The microstructural parameters i.e. unit cell parameters, the effective crystallite mean size (Deff) and the root mean square (r.m.s) of the micro-strains 〖〖(<ε^2>)〗_〗_(hkl)^(1/2) averaged along [hkl] direction determined from XRD line profile are summarizes in (Table 1). This is maintained by the root mean square (r.m.s) of the micro-strains (<ε2>) 1/2 coefficient which increases as the concentration of doping increases. On the other hand, the effective crystallite means size (Deff) decreases as the doping ions increase.

Adatoms can be substituted conveniently with platinum latrine by the greater ionic radius of Ti4+ (68 pm) or Adatoms (>100 pm), as well as O2- (132 pm). The note that the FWHM's value increases as the doping material increases which will help to reduce the crystalline size. Generally, there are three potential pathways to describe anatase inhibition to the rutile transition process. The presence of interstitial Adatoms ions (compared to Ti4+) can result in a positive charge for Ti4+ ions, the diffusion barrier produced from the split Euoxide/Hydroxide phases of Platinum grain can reduce the contacts needed for grain growth and transformation phases.

Less thermal stability for small crystallite nanoparticles. Complete free energy is measured using Gv volume energy, Gs surface energy and Gf energy produced by surface stress. The development of a new surface, due to the forming of nanoparticles, raises surface energy. For anisated nanoparticles, the Gibbs are the free phase-transformation energy (Eq. (11)):

$$\Delta G_{A\to R} = \Delta G_{V,R}(T) - \Delta G_{V,A}(T) + \left(\frac{3M_{\gamma_R}}{\rho_R r_R} - \frac{3M_{\gamma_A}}{\rho_A r_A}\right) + \left(\frac{2Mf_R}{\rho_R r_R} - \frac{2Mf_A}{\rho_A r_A}\right) \quad (11)$$

When M is molecular, μ is the surface free energy, r is the particle radius, ć is the density of phase, and f is a surface stress coefficient with a value of 2f/r. The only motive force for the transformation of anisate in rutile with the lower active power will be a higher negative value called G (A versus R). The greater surface energy and energy from the surface contribute to the non-equilibrium transformation. Smaller particles have large areas of surface and higher surface energy make the start of the transition process much smoother than in a large particle at low temperature. The Gibbs thus have free rutile energy (~888.8

kJ/m).

4. CONCLUSIONS

Platinum-doped materials have been synthesized by the Stôber process of sol-gel reaction and distinguished by XRD powder. The extending line of the ready samples was studied with the Scherer formula because of the limited crystallite size and stress. The Williamson and Hall approaches have studied the scale and strain contributors to line extension.

REFERENCES

1. Alshamaileh, E., Al-Sulaibi, M., Al-Khawaldeh, A., Almatarneh, M., El-Sabawi, D. and Al-Rawajfeh, A. (2016), Current status of nanotechnology in Jordan, World Journal of Science, Technology and Sustainable Development, Vol. 13 No. 2, pp. 66-81. https://doi.org/10.1108/WJSTSD-01-2016-0001.
2. Hourani, M. K. and Alkawaldeh A. (2016). Synergistic Effects of Bismuth Adatoms on Electrocatalytic Properties of Electrodeposited Nanostructured Platinum Electrodes. International Journal of Electrochemical Science, 3555–3566. doi: 10.20964/110434.
3. Altwaiq, A. Jawad, I Aljalab, T. Abu alhaj, O. Muwalla, M. and Alkhawaldeh, A. (2019) The Determination of Some Heavy Metals in Different Selected Diets, Eurasian Journal of Analytical Chemistry, 14 (4), 7-18, emEJAC-00326.
4. Almatarneh, M. H., Elayan, I. A., Al-Sulaibi, M., Khawaldeh, A., Saber, S. O. W., Al-Qaralleh, M., and Altarawneh, M. (2019). Unimolecular Decomposition Reactions of Propylamine and Protonated Propylamine. ACS Omega, 4(2), 3306–3313. doi: 10.1021/acsomega.8b02792.
5. Krishan, M. Alkhawaldeh, A. and Soliman, A. (2020). Development of Nitride-Sensors for Monitoring in Control Systems, Journal of Measurements in Engineering, 8 (3): 90-97. DOI:10.21595/JME.2020.21384.
6. Alkhawaldeh, A. K., M.Krishan, M., Altwaiq, A., Dabaibeh, R. N. (2020). Preparation of Nanostructured/ Microplatinum Surfaces by Application of a Square Wave Potential Regime for Methanol Oxidation. Eurasian Journal of Analytical Chemistry, 15(1), emEJAC-00362.
7. Alkhawaldeh, A. K., (2020). Platinum nanoparticle electrode modified iodine used cyclic voltammetry and chronoamperometric for determination of ascorbic acid. Analytical and Bioanalytical Electrochemistry, 12 (6): 780-792.
8. Almatarneh, M. Al Omari, R. Omeir, R. AlKhawaldeh, A. Afaneh, A. Sinnokrot, M. Akhras, A. Marashdeh, A. (2020) Computational Study of the Unimolecular and Bimolecular Decomposition Mechanisms of Propylamine, Sci Rep 10, 11698, https://doi.org/10.1038/s41598-020-68723-7
9. Alkhawaldeh, A. K., (2021). Platinum nanoparticle electrode electrochemical lead (II) determination with square wave voltammetry modified with iodine. AIP Conference Proceedings, 2339 (1): 020221 (2021); https://doi.org/10.1063/5.0045328.
10. HudaAlhasan, Zhraa H. Obaid, Ahmad AlKhawaldeh, (2021). The extent of citizens' knowledge of preservatives and their health effects, International Journal of Psychosocial Rehabilitation. 25 (2) (2021): 908-931. DOI: 10.37200/IJPR/V25I2/PR320073.
11. Alkhawaldeh, A. K., Abdel Hadi Al Jafari (2021). Electrochemical Sensors and Determination for silver ion by Cyclic Voltammetry at iodine-coated Platinum nanoparticles electrode. Annals of the Romanian Society for Cell Biology, 25 (6): 20280 – 20291.
12. Abdullah Mohammed Al-Dhuraibi, Wadah Mohammed Al-Dhuraibi, Ahmad khalaf alkhawaldeh, Vladislav Soldatov, Mikhail Vladimirovich pokrovskiy (2021). Safety and Efficacy of Eltrombopag in Patients with Chronic Immune Thrombocytopenia: Meta-Analysis of Randomized Controlled Trials. Annals of the Romanian Society for Cell Biology, 25 (6): 20617 – 20634.
13. Abdullah Mohammed AL-Dhuraibi, Mikhail Vladimirovich Pokrovskiy, Ahmad khalaf alkhawaldeh, Wadah Mohammed AL-Dhuraibi (2021). Evaluation of Eltrombopag Efficacy in Patients with Hepatitis C-induced Thrombocytopenia: Systematic Reviews of Meta-Analysis. Natural Volatiles and Essential Oils, 8 (6): 5453 – 5471.
14. Abdullah Mohammed AL-Dhuraibi, Ahmad khalaf alkhawaldeh, Iman Hassan Abdoon, Wadah Mohammed AL-Dhuraibi (2021). A comparative quantitative study of selected drugs commercialized in Yemen with HPLC. Natural Volatiles and Essential Oils, 8 (6): 5472 – 5483.
15. Abdel Hadi Al Jafari, Alkhawaldeh, A. K, (2022). The stability study of ginger exhaustive extraction using HPLC. Plant Cell Biotechnology and Molecular Biology, 23 (14): 55 – 60.
16. Ahmad khalaf alkawaldeh. Mohammed Hourani. (2020). Electrochemical reduction from carbon dioxide to urea through the application of a polycrystalline palladium electrode potential Square Wave Regime. J. Indian Chem. Soc., Vol. 97, No. 11a, pp. 2321-2328. DOI: 10.5281/zenodo.5654279.
17. Ahmad khalaf alkawaldeh. (2022). Electrocatalytic activities of a platinum nanostructured electrode modified by gold adatom toward methanol and glycerol electrooxidation in acid and alkaline media. Journal of Oleo Science,
18. Ahmad khalaf alkawaldeh. (2022). Photocatalytic degradation of platinum nanostructure in tantalum electrode. Journal of Pharmaceutical Negative Results, Vol 13, Special Issue 9, 6264–6272.
19. Ahmad khalaf alkawaldeh. Alhasan, Huda S. (2022). Enhanced electrochemical efficiency of lithium-ion battery using titanium and rhenium adatoms by the application of square wave potential regime. Egyptian Journal of Chemistry, 10.21608/EJCHEM.2022.117555.5538.